

A Study of $\text{Ce}_x\text{Fe}_{1-x}\text{O}_2$ as a Reducible Oxide for the Thermal Hydrogen Production from Water

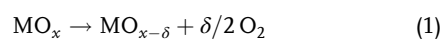
Salem Al-Taweel, M. A. Nadeem, and Hicham Idriss*

Thermal water splitting over 1550 °C-reduced CeO_2 and $\text{Ce}_{0.95}\text{Fe}_{0.05}\text{O}_{2-\delta}$ is studied. Hydrogen production over $\text{Ce}_{0.95}\text{Fe}_{0.05}\text{O}_{2-\delta}$ was found to be equal to $2.53 \times 10^{-4} \text{ mol}(\text{H}_2) \text{ g}_{\text{oxide}}^{-1}$ which is higher than that observed on CeO_2 . The reaction kinetics for $\text{Ce}_{0.95}\text{Fe}_{0.05}\text{O}_{2-\delta}$ is also found to be faster. The oxides are studied by X-ray diffraction, temperature programmed reduction, and scanning transmission electron microscopy (STEM). XRD results show that Fe is substituted for Ce^{4+} in the as prepared oxides. Fe^{3+} cations substitution also decreases the CeO_2 crystallites size. Heating to 1100 °C increases their size, although the Fe-containing oxide still shows smaller crystallites when compared with CeO_2 alone. The activation energy for surface reduction of CeO_2 , extracted from TPR, is found to be slightly higher (1.58 eV) than that of bulk reduction (1.43 eV). While high resolution TEM and electron energy loss spectroscopy before reaction show that Fe cations are homogeneously distributed, those after reaction show in addition to the growth of the crystallites size, Fe segregation to the edges of the crystals, although no detachment of Fe oxide particles is seen. The mechanism of water dissociative adsorption and hydrogen re-combinative desorption is discussed in which the role of Ce–O–Fe sites is considered.

1. Introduction

Solar thermal hydrogen production from water (often called thermochemical water splitting [TCWS]) using reducible oxides has been studied for a few decades.^[1–3] The principle relies on two sets of reactions. The first one is an endothermic reaction where an oxide in a binary or multiple phases is reduced at a high temperature in inert environment releasing molecular oxygen. Temperatures as high as 1500 °C are typically needed. The second one is an exothermic reaction in which the reduced oxide

material is exposed to water vapor, typically a few hundred degrees lower in temperatures. In this second step, the reduced oxide is oxidized back and molecular hydrogen is released. In other words, molecular hydrogen and oxygen are produced separately. The following two simplified equations present the two steps.



where M is a metal cation such as Ce^{4+} cation, x is for the compound stoichiometry (2 in the case of CeO_2) and $\delta < x$ (typically a small fraction of x).

The fact that it uses the entire solar spectrum puts it among the highest systems for hydrogen generation from water if not the highest.^[4] Many cycles^[5] have theoretical efficiencies >40% and while it is still in the research phase, it has a potential to be constructed at large scale for practical uses.

A few systems are commonly investigated, these include perovskites based,^[6,7] hercynites,^[8,9] and fluorite based oxides.^[10,11] Among the most studied fluorite base oxides is CeO_2 because of its fast kinetics^[12] in addition to its stability during the redox cycles.^[13] Yet, the high temperature required for its partial reduction (mostly, but not totally, because of the high energy for the “oxygen vacancy formation”, typically above 3 eV^[14]) makes it unpractical.^[15] This has motivated many researchers to modify its properties to destabilize the Ce–O bonds and therefore decrease the formation energy of oxygen vacancies.^[16] Three methods are often used to do this. 1) Compensation for lattice expansion, where a fraction of Ce^{4+} cations is substituted by a smaller size M^{4+} such as Zr^{4+} cations.^[17] 2) Charge transfer where a fraction of Ce^{4+} cations is substituted by a metal cation that can donate electrons and in the process becomes more oxidized such as U^{4+} cations.^[18] 3) Aliovalent doping, where also a fraction of Ce^{4+} cations is replaced by metal cations; often in a lower oxidation state than +4, this results in the decrease in oxygen concentration in the lattice and consequently creating “noncharged” oxygen vacancies in the fluorite structure.^[19] While this does not cause additional reduction, it can cause enough distortion to change the energetics of the redox system favorably.^[20]

Among the aliovalent systems, making a solid solution of CeO_2 that contains Fe^{3+} has been studied in some details. In one of these works it was found that substituting a fraction of Ce^{4+} by Fe^{3+} cations in CeO_2 led to a decrease in the activation

S. Al Taweel, M. A. Nadeem, H. Idriss^{[+],[++]}
Surface Science and Advanced Characterization Department
SABIC Corporate Research Center at King Abdullah University of Science and Technology (KAUST)
23955 Thuwal, Saudi Arabia
E mail: h.idriss@ucl.ac.uk, idriss@sabir.com

^[+]Present address: Institute of Functional Interfaces, KIT, 76344 Karlsruhe, Germany

^[++]Present address: Department of Chemistry, University College London, WC1E 6BT London, UK

energy for the selective catalytic reduction reaction of NO by half.^[21] This seems to have resulted from the formation of a distorted Fe—O—Ce structure. Density functional theory (DFT) calculation and titration via pyridine adsorption indicated that this Fe—O—Ce structure has increased the number of Lewis acid sites as well as the charge density around Ce⁴⁺ cations when compared with those of pure CeO₂. The authors also found that their formation mechanism is related to the Fe content. Low Fe fraction ($x < 0.3$) kept the fluorite structure (solid solution) via a vacancy compensation mechanism, leading to an increase in oxygen vacancies which, in turn, increased the catalytic performance. Other work has shown that the X ray photoelectron spectroscopy (XPS) Ce3d lines of Ce cations have considerable Ce³⁺ presence at ≈ 885 and 904 eV (V' and U' lines) upon the introduction of Fe³⁺ cations into the lattice of Ce_{0.8}Fe_{0.2}O_x^[22] ($x = 2 - \delta$, where δ is deviation from stoichiometry) or up to when Ce and Fe are of equal proportions.^[23]

The incorporation of Fe³⁺ cations into the fluorite structure of CeO₂ has also been studied by X ray diffraction (XRD) among other methods. Crystalline CeO₂ gives rise to strong lines at $2\theta = 28.5^\circ$, 33.0° , 47.5° , and 56.4° for the (111), (200), (220), and (311), respectively, whose positions and full width half maximum (FWHM) being sensitive to its crystallite dimension and degree of crystallinity. Hematite Fe₂O₃ gives lines at $2\theta = 33.3^\circ$, 35.7° , and 62.3° for the (104), (110), and (214) lines. Because Fe³⁺ (0.6 Å) ions are much smaller than Ce⁴⁺ ions (≈ 1 Å in octahedral coordination), their incorporation into the lattice can be monitored mostly by a positive shift of 2θ which is often associated with a broadening of the lines due to the formation of smaller crystallites.^[24] Therefore, both the shift and the absence of Fe₂O₃ lines are often taken as a strong indication of the presence of a solid solution. Depending on the preparation method, this is found up to about 0.3–0.4 atomic ratio Fe³⁺/Ce⁴⁺ cations.^[17–25]

The increased reduction of CeO₂ was also studied by temperature programmed reduction (TPR) by others. Pure CeO₂ is reduced in two temperature domains at about 500 and 800 °C.^[26] The first has been attributed to surface reduction while the second to bulk reduction. The reduction is weak (leads to the removal of a small fraction of oxygen anions typically 10%–20%) and the formation of Ce³⁺ cations within the investigated temperatures in TPR (typically up to 1000 °C). Pure Fe₂O₃ is reduced largely to metallic Fe with a single dominant peak corresponding to bulk reduction. The incorporation of Fe cations into CeO₂ increases the reduction process (increased hydrogen consumption during TPR) together with decreasing the reduction temperature, in particular that of the first peak of CeO₂ which is often split into multiple ones. Only few thermogravimetric analysis (TGA) experiments of doped CeO₂ with Fe cations were conducted. In a one particular study devoted to the effect of doping CeO₂ with metal cations, it was found that the incorporation of Fe³⁺ increased the mass loss of CeO₂ (due to reduction). In this case for Ce_{0.9}Fe_{0.1}O_{2– δ} , 50.0 μmol of O₂ g_{material}^{–1} was removed at each cycle during ten thermochemical cycles in which the thermal reduction step was performed at 1400 °C. These were active sites because nearly stoichiometric CO production (by CO₂ reduction) 96.3 μmol g_{material}^{–1} · cycle at 1000 °C^[23] was seen.

TCWS is still in the research phase with only limited demonstrations available. The main issue is the very high temperature needed requiring expensive solar concentrators and associated reactor materials and the stability of the oxide (or mixed oxides) used to withstand the thermochemical cycles.^[27]

In this work, we have investigated the redox properties of CeO₂ alone and when doped with Fe³⁺ with a 0.05 and 0.25 stoichiometric ratios with respect to Ce⁴⁺ cations mostly by TPR, XRD, and transmission electron microscopy (TEM) in addition to water splitting.

2. Results

2.1. XRD

Figure 1 shows the XRD patterns of CeO₂, Ce_{0.95}Fe_{0.05}O₂, and Ce_{0.75}Fe_{0.25}O₂ oxides that were heated at the indicated temperatures.

A typical diffraction pattern of CeO₂ with nano size dimension is seen for the “as prepared” oxide, with size of about 14 nm and lattice parameter (**a**) of 0.543 nm (**Figure 1A**). Heating does not induce much changes in both parameters up to about 900 °C, where an abrupt change occurs. At this temperature the crystallite size (**L**) considerably increased (sintering) together with an increase in the cubic lattice parameter (**a**) (due to bulk reduction). This has occurred twice, at 900 °C where **L** increased to 39.4 nm and **a** to 0.545 nm and at 1100 °C where **L** doubled to 80.2 nm and a further expansion of **a** (0.546 nm) is noted. In the case of Ce_{1– x} Fe _{x} O₂, data suggest that the addition of Fe to CeO₂ is substitutional because no other diffraction lines attributed to Fe₂O₃ were seen up to 900 °C or so. The crystallite size decreased considerably, more so in the case of Ce_{0.25}Fe_{0.25}O₂ than Ce_{0.95}Fe_{0.05}O₂ where **L** decreased to about 6 nm. Also, **a** decreased when compared with that of CeO₂ (0.540 nm). There is a gradual increase in 2θ which is also an evidence of incorporation of Fe³⁺ into the fluorite lattice upon substitution of Ce⁴⁺. Overall, a similar behavior to CeO₂ with respect to temperature is seen in the case of Ce_{1– x} Fe _{x} O₂ albeit with one noticeable difference. A gradual and not abrupt lattice expansion is noted in both Fe containing oxides. It is, however, clear that some segregation occurred at 1100 °C because diffraction lines corresponding to Fe₂O₃ (110) and (003) were observed. **Table 1** compares the parameters of the three oxides at 500 and 1100 °C.

2.2. TPR

Figure 2 shows TPR of the as prepared CeO₂ that has been calcined at different temperatures. The Brunauer Emmett Teller (BET) surface area is indicated on the left hand side while the hydrogen consumption is indicated closer to the observed peaks. CeO₂ calcined at 500 °C showed two domains with a total hydrogen consumption of 19.2 mL g^{–1}. Increasing the calcination temperature by 30 °C resulted in a decrease in the ratio of the two peaks in favor of the high temperature one, while the overall hydrogen consumption remained similar. Further increasing the calcination temperature decreased the first peak. The first peak has completely disappeared for the 700 °C calcined sample (and still the total amount of hydrogen consumed is equal

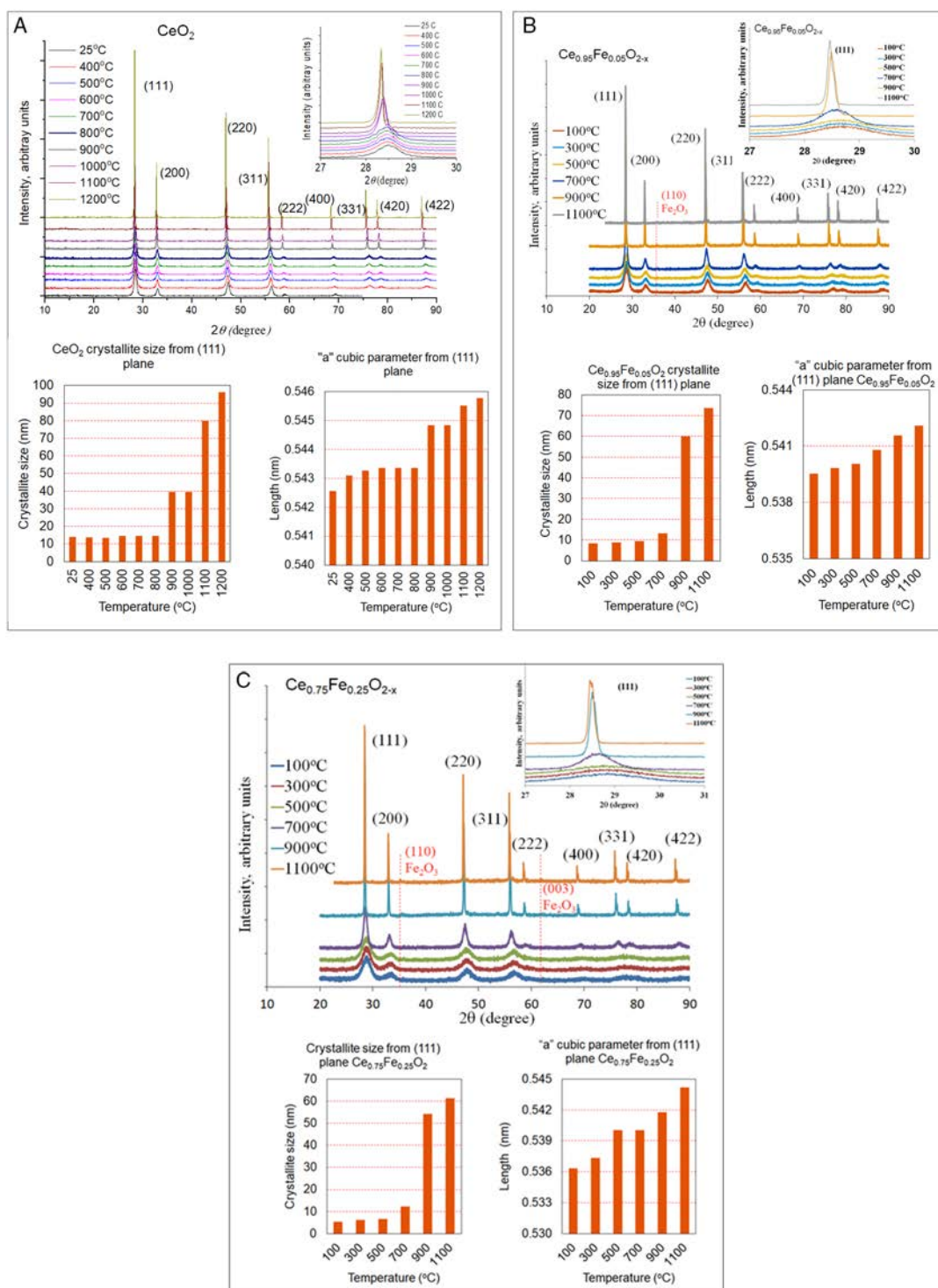


Figure 1. A) XRD patterns of as prepared CeO_2 in the $10-90^\circ$ range together with the extracted crystallite size and cubic parameter from the (111) lines, the inset in the XRD pattern is a zoom on the (111) diffraction line to highlight the shift in angle and narrowing of the FWHM with increasing temperature in ambient environment. Similar results for B) $\text{Ce}_{0.95}\text{Fe}_{0.05}\text{O}_2$ and C) $\text{Ce}_{0.75}\text{Fe}_{0.25}\text{O}_2$ oxides.

to that of the sample calcined at 500°C). Higher calcination temperatures (not shown) were also studied up to 900°C and all showed one peak in the $800-900^\circ\text{C}$ temperature domain at the ramping rate of $10^\circ\text{C min}^{-1}$. The disappearance of the first

peak together with the considerable decrease in the BET surface area and the constant consumption (within analytical errors of peak computation) all point out to the attribution of the first peak to surface reduction and the second one to that of bulk reduction.

Table 1. Crystallite size and cubic lattice dimension for CeO₂ and Ce_{1-x}Fe_xO₂ at 500 and 1100 °C. Data extracted from Figure 1.

Oxide	2θ CeO ₂ (111), degree at 500 °C	Crystallite size at 500 °C [nm]	Cubic lattice parameter at 500 °C [nm]	Crystallite size at 1100 °C [nm]	Cubic lattice parameter at 1100 °C [nm]
CeO ₂	28.46	14	0.543	80.2	0.545
Ce _{0.95} Fe _{0.05} O ₂	28.68	9.5	0.540	73.6	0.542
Ce _{0.75} Fe _{0.25} O ₂	28.84	6.5	0.540	61.3	0.544

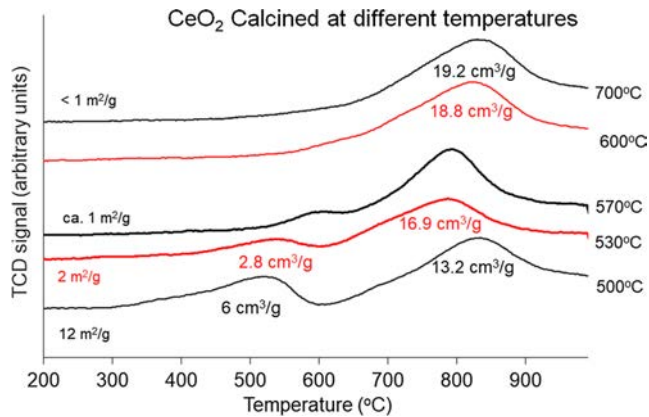


Figure 2. TPR of polycrystalline CeO₂ that was prior calcined at the indicated temperatures (from 500 to 700 °C). The normalized BET surface area and amount of consumed hydrogen (in cm³ g⁻¹) are also indicated. Note the gradual disappearance of the first peak with increasing calcination temperature.

An estimation of the surface reduction can be made from the BET surface area knowing that the CeO₂ surface is predominantly (111) which is oxygen terminated^[28] and that in 1 m² there is about 1 × 10¹⁹ atoms of oxygen (or ≈1.2 × 10²⁰ atoms for the 12 m² g⁻¹ of CeO₂). The TPR of the 500 °C calcined CeO₂ resulted in the consumption of ≈1.6 × 10²⁰ molecules of hydrogen for the first peak. In other words it appears that all surface oxygen atoms were removed. From the total amount of hydrogen consumed one can have an estimation of the O to Ce ratio upon H₂ reduction during TPR; it was found to be CeO_{1.85}.

To gauge the energy needed to remove these oxygen atoms during TPR, one can calculate the activation energy for each peak. This can be conducted by changing the ramping rate and applying the two methods indicated in the experimental section. The data are shown in **Figure 3**. Both methods (Redhead and Kissinger) gave similar activation energies for reduction. The surface reduction had an activation energy of 150–160 kJ mol⁻¹ (≈1.6 eV), while the bulk reduction was found slightly smaller (135–145 kJ mol⁻¹ [≈1.45 eV]). For comparison, the computed (using DFT + U_{eff} = 5 eV) oxygen vacancy formation energy for reduction of CeO₂(111) was conducted by others.^[29] A similar trend has been found, a slightly higher energy for surface reduction than that of bulk reduction (**Table 2**).

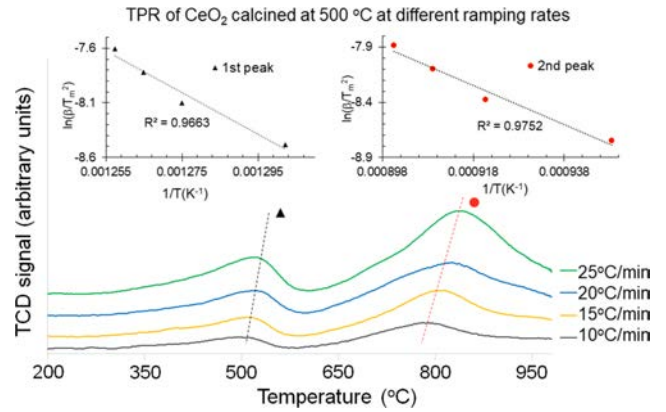


Figure 3. TPR of polycrystalline CeO₂ calcined at 500 °C at ramping temperatures, β, equal to 10, 15, 20, and 25 °C min⁻¹. The insets show the plot of Ln β/T_m² as a function of 1/T where T_m is the maximum peak temperature (using Equation (2), as indicated in the Experimental Section).

Next, TPR of Ce_{1-x}Fe_xO₂ together with that of Fe₂O₃ was conducted (**Figure 4**). The four profiles are plotted as monitored without multiplication but with offset for clarity. The amount of oxide used is given on the left side of each profile and the total amount of consumed hydrogen is given on the right side. The stoichiometry of the oxides, based on their formulae units, is given next to each line. The table in the inset presents the stoichiometry based on hydrogen consumption (loss of oxygen) as extracted from TPR. Fe₂O₃ is expected to be completely reduced to metallic iron. The theoretical amount of hydrogen to reduce it (≈420 mL g⁻¹) is about 80% of that observed (Fe₂O₃ + 3 H₂ → 2 Fe + 3 H₂O), while close it indicates that experimental errors of 20% or so are to be taken in consideration for the other oxides. The results of the mixed oxides can be qualitatively explained based on those obtained from the pure ones. The two peaks of CeO₂ that are labeled I and II represent surface and bulk reductions, as presented earlier. Based on XRD (and TEM later) results, the addition of Fe to CeO₂ is substitutional and resulted in decreasing the crystallite size. The decrease in crystallite size would, in turn, result in increasing the surface to bulk ratio which explains the increase in peak I compared with peak II ratio in the CeFe oxides. Peak III is that of pure Fe₂O₃; because it is also present in the case of Ce_{0.75}Fe_{0.25}O₂ some Fe cations may have segregated out of the fluorite structure. The increase in peak II of CeFe oxides compared with CeO₂ alone might be due to the ease of bulk reduction due to the presence of Fe cations inside the fluorite structure.

Table 2. Activation energy for surface and bulk reduction extracted from TPR experiments.

CeO ₂	Experimental Redhead ^[25] [eV]	Experimental Kissinger ^[26] [eV]	Computation (DFT + U) CeO ₂ (111)—unstrained ^[29] [eV]
Surface [eV]	1.65	1.58	2.1
Bulk [eV]	1.52	1.43	1.9

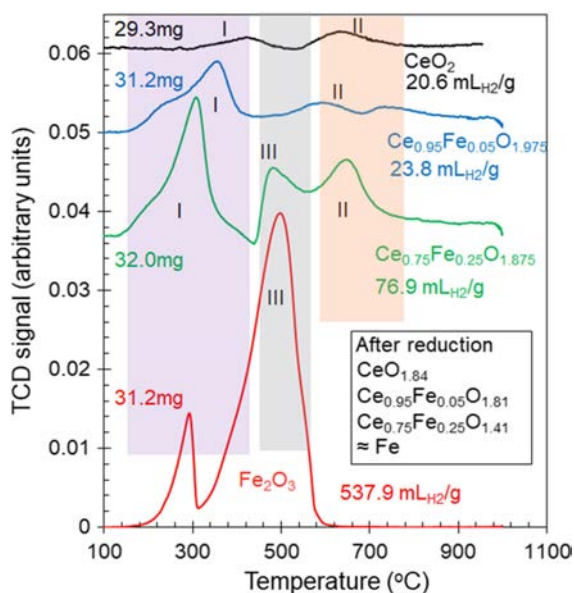


Figure 4. TPR of CeO_2 , $\text{Ce}_{0.95}\text{Fe}_{0.05}\text{O}_{2-\delta}$, $\text{Ce}_{0.75}\text{Fe}_{0.025}\text{O}_{2-\delta}$, and Fe_2O_3 . All oxides were precalcined at 500°C . The computed values of $2-\delta$ are given beside each line in the formulae units. The inset rectangle has the computed formulae units based on the oxygen loss during TPR. The amount of hydrogen used to fully reduce Fe_2O_3 to Fe gives an indication on the errors, about 20%. The highlighted regions I and II are those of surface and bulk reduction of CeO_2 while region III is that of bulk reduction of Fe_2O_3 . The first peak in the TPR of Fe_2O_3 might be due to surface reduction.

2.3. TEM

Figure 5 shows the TEM, selected area electron diffraction (SAED), and energy dispersive X ray (EDX) of $\text{Ce}_{0.95}\text{Fe}_{0.05}\text{O}_{2-\delta}$ and $\text{Ce}_{0.75}\text{Fe}_{0.025}\text{O}_{2-\delta}$ results that were calcined at 500°C . Both present the fluorite structure of CeO_2 ; no Fe_2O_3 phase was seen. The d spacing of the fluorite structure shows a slight decrease in the case of $\text{Ce}_{0.75}\text{Fe}_{0.025}\text{O}_{2-\delta}$ when compared with $\text{Ce}_{0.95}\text{Fe}_{0.05}\text{O}_{2-\delta}$ which also matches the polycrystalline XRD data (Figure 1). Therefore, both microscopic and macroscopic diffraction methods indicate that the crystallite size of CeO_2 decreases with Fe substitution. From TEM the average crystallite size of $\text{Ce}_{0.95}\text{Fe}_{0.05}\text{O}_{2-\delta}$ is 8–10 nm, while that of $\text{Ce}_{0.75}\text{Fe}_{0.025}\text{O}_{2-\delta}$ is 5–7 nm. Decreasing the crystallite size means that the surface energy has decreased (more stable) when compared with that of CeO_2 . EDX shows the presence of Fe in both mixed oxides with an intensity tracking the expected concentration.

2.4. Thermal Water Splitting

Figure 6 shows the activity of reduced CeO_2 and reduced $\text{Ce}_{0.95}\text{Fe}_{0.05}\text{O}_{2-\delta}$ for thermal water splitting at 1200°C , while Figure 7 shows the STEM, EDX, and electron energy loss spectroscopy (EELS) results of the $\text{Ce}_{0.95}\text{Fe}_{0.05}\text{O}_{2-\delta}$ oxide after the reaction. The oxides were heated to 1550°C for 120 min. The incorporation of Fe ($\text{Fe}/\text{Ce} = 0.05$) into CeO_2 has resulted in two main effects. The kinetic of the hydrogen production has

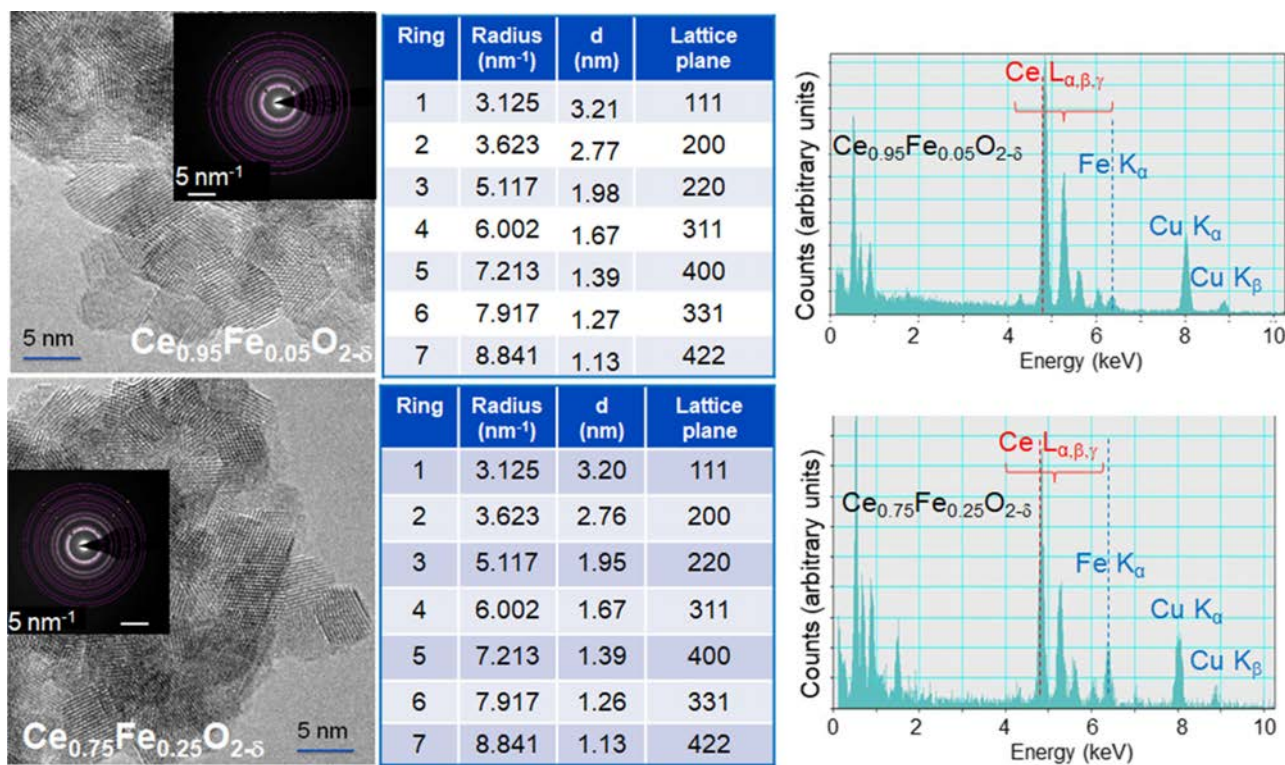


Figure 5. TEM, SAED, and EDX of $\text{Ce}_{0.95}\text{Fe}_{0.05}\text{O}_{2-\delta}$ and $\text{Ce}_{0.75}\text{Fe}_{0.025}\text{O}_{2-\delta}$ that were calcined at 500°C . The values in the table in the middle are extracted from the SAED in the inset of the TEM images and ring numbers start with the center of the concentric circles (the bright spot of each inset).

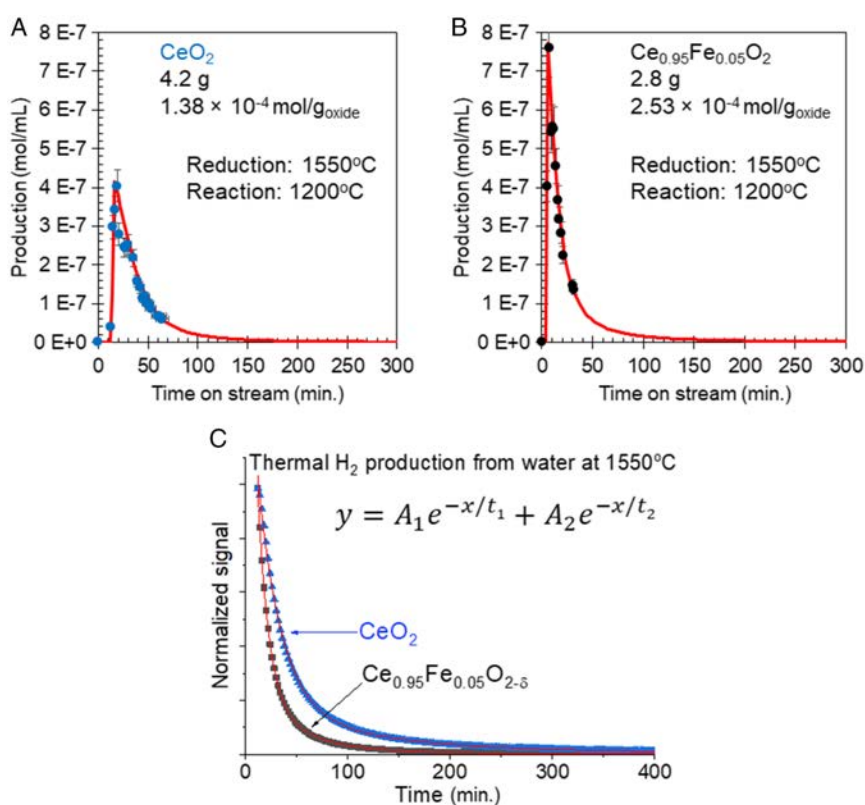


Figure 6. Thermocatalytic water splitting over A) CeO_2 and B) $\text{Ce}_{0.95}\text{Fe}_{0.05}\text{O}_{2-\delta}$ at 1200 °C; the oxides were reduced under N_2 at 1550 °C for 2 h prior to use. The total amount of hydrogen from water per g of oxide is indicated. C) Normalized fitting of the decay part of H_2 production using a biexponential function for both oxides.

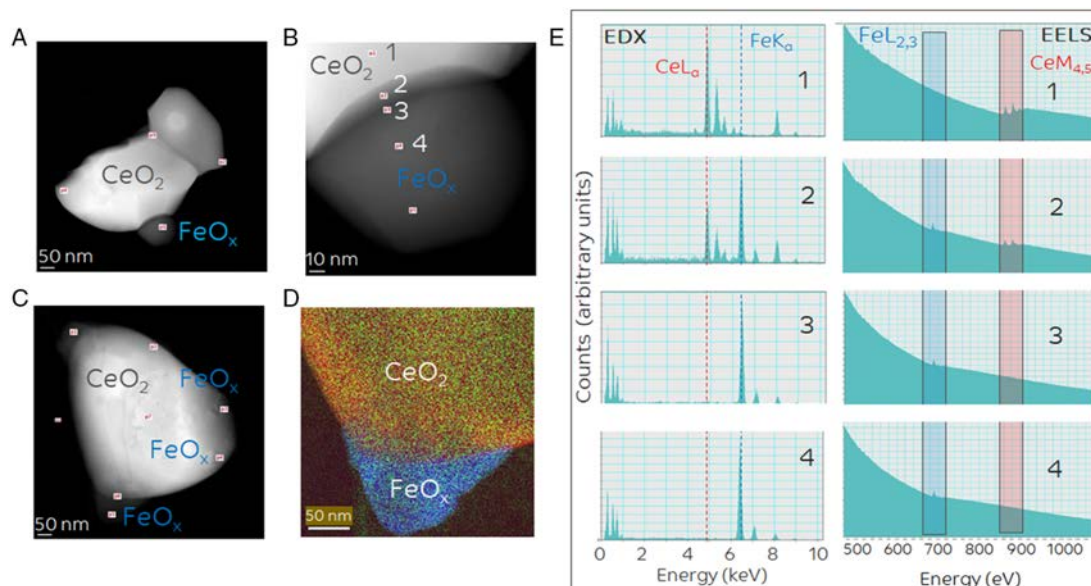


Figure 7. STEM, EDX, and EELS of $\text{Ce}_{0.95}\text{Fe}_{0.05}\text{O}_{2-\delta}$ after the reaction presented in Figure 6. A,B) One particle and C,D) another particle. D) An elemental EELS map of the particle in (C). E) The numbers 1–4 are those labeled in (B). While clear segregation of iron to the edges of CeO_2 is seen, some iron is still present (EDX) within the crystallite (also note the presence of FeO_x on the large CeO_2 crystallite in C). The crystallite size as observed with TEM is close to 1 μm (an increase in almost 200 times when compared with that calcined at 500 °C). Yellow for cerium, blue of iron, and red for oxygen atoms. Based on elemental mapping, it seems that FeO_x is highly deficient in oxygen.

increased and the total amount has almost doubled (per unit weight of oxide). This is in line with the expected results because most studies including this one have pointed out to an increased reduction of CeO₂ due to the presence of Fe cations (up to a threshold level).^[19–25] The FWHM of the production peak decreased from ≈35 to about 10 min (Figure 6A,B) which gives a simple observation on the kinetic effect. To further see the effect of Fe on the reduction kinetics, the decay part of the peaks was fitted with an exponential decay function. Attempts with a single exponential decay fit were not successful, yet a double exponential fit was found to be perfect with R² of 0.999. **Table 3** shows the different parameters of the decay for both oxides. The addition of Fe has increased the time constant (in min⁻¹) for water splitting by a factor of 2 when compared with CeO₂ alone. However, increasing the number of reduced sites, in principle, should not reduce the decay time but mostly affect the amplitude (prefactors A₁ and A₂) if these sites are all of similar nature and do not interact with each other. The increase in the time constant by a factor of two in the case of the Fe doped CeO₂ indicates that the reduced sites are more reactive than those of CeO₂ alone (see further discussion later). The ratio t₁/t₂ (or τ₂/τ₁) was found to be almost the same for both oxides. It is not simple to attribute a separate physical meaning to both decay constants. While, as shown in Figure 7, the used oxide is not homogenous (Fe oxide segregation occurs) because the ratio of the time constants is the same for the pure CeO₂, it is tempting to attribute the slowest (t₂) decay to events requiring more (or additional) energy than the first one; such as defects diffusion from the bulk to the surface (or vice versa). Initially, defects are statistically distributed in the bulk and on the surface, and then with the progress of the reaction more and more defects are healed; this will decrease the reaction rate because a defect site (or a bulk oxygen atom) would need to travel longer distance to reach the surface. In other words, the first decay might be largely independent from the defects distribution while the second decay would be.

The activation energy for oxygen diffusion in CeO₂ is typically a small fraction from that needed to reduce it (about 10% or so or 0.3 eV).^[30] It is worth indicating that in the process of oxidation of the reduced CeO₂ with water vapor two important chemical steps occur. These are water dissociative adsorption and oxygen anions diffusion from the surface to the bulk (or defects diffusion from the bulk to the surface). The first one is different on a stoichiometric surface when compared with defected ones and therefore their kinetic effect on the reaction is expected to be different. It has been found computationally that water dissociative adsorption over reduced CeO₂ has a stronger energy than that on stoichiometric surface.^[31] As shown in Figure 7, the particles have considerably sintered during the reduction process so intraparticle pore diffusion of water molecules can be neglected. Although the considerable increase in the volume to surface ratio upon sintering makes the process mostly bulk driven (as the majority of the

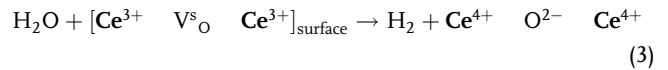
oxygen defects would be located in the bulk), the reaction would still be surface driven first if the adsorption of water is a limiting step. While a fraction of Fe oxides has segregated out, there is still some Fe inside as seen by EDX and EELS (Figure 7). It is therefore also possible that, in some locations, the interface has the needed gradient concentration of Fe cations to positively affect the reaction rate when compared with pure CeO₂.

The three following equations summarize the main reactions that occur during water oxidation. Strictly, large crystallites of CeO₂ are (111) O terminated and in the fluorite structure and these terminated oxygen anions are bonded to three Ce cations in the second layer, yet for the sake of simplicity it is easier to write them as (Ce—O—Ce) bearing in mind that they are not in the same plane.

2.5. Reaction Steps

2.5.1. Electron Transfer Reaction

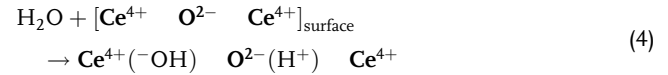
Water dissociative adsorption on surface oxygen defect followed by oxidation.



V_O^s is for a surface oxygen defect and Ce³⁺ is for a reduced cation in the second layer of the (111) terminated surface.

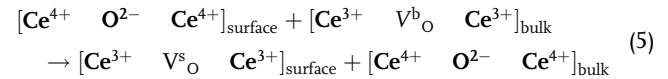
2.5.2. Acid Base Interaction

Water dissociative adsorption over a stoichiometric sites (note that there is no charge transfer)



2.5.3. Diffusion

Surface oxygen diffusion into the bulk (or defect diffusion into the surface) driven by heat and water dissociative adsorption (Equation (3) and (4)).



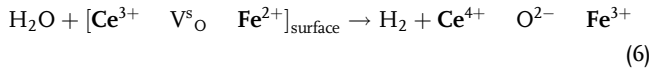
V_O^b is bulk oxygen defect.

The two protons in Equation (4) (of the two surface hydroxyls) become one molecule of hydrogen upon the reaction with two electrons from Equation (5).

Table 3. Fitting parameters for the decay part of the hydrogen production profile (at 1200 °C) from water as a function of time of the prereduced oxides at 1550 °C. The time constant τ = 1/t. A double exponential decay equation was used γ = A₁e^{-x/τ₁} + A₂e^{-x/τ₂}.

Oxide	A ₁ [mol mL ⁻¹]	t ₁ [min]	τ [min ⁻¹]	A ₂ [mol mL ⁻¹]	t ₂ [min]	τ [min ⁻¹]	t ₁ /t ₂
CeO ₂	7.3 × 10 ⁻⁷	22.5 ± 0.2	0.044	9.7 × 10 ⁻⁸	108.8 ± 2.9	0.009	0.21
Ce _{0.95} Fe _{0.05} O ₂	1.2 × 10 ⁻⁶	10.7 ± 0.06	0.093	1.3 × 10 ⁻⁷	47.3 ± 0.6	0.021	0.23

It is possible that the substitution of a fraction of Ce cations by Fe cations on the surface and in the bulk affects Equations (3) and (5). Equation (4) is a simple acid–base exchange reaction that would be less affected by the change in the nature of a metal cation. Although it can be affected by the degree of coordination^[32] (such as in different surface structures), this is neglected here because of the small energy difference. Based on the results shown in Figure 6, the concentration of V_O has increased in the presence of Fe cations and this affects primarily Equation (1). However, the faster kinetics indicate that the dissociative adsorption of water on oxygen vacancy sites is also accelerated when Fe cations are present. Therefore, for doped CeO_2 Equation (6) below is expected to be faster than Equation (3) if at least the dissociative adsorption energy is higher on $Fe-V^s_O-Ce$ when compared with $Ce-V^s_O-Ce$ centers. It is also important to point out that recent computation and experimental studies have also pointed out to the role of H_2 formation as the rate limiting step of the reaction.^[30]



3. Conclusions

The thermochemical water splitting at 1200 °C over reduced CeO_2 and $Ce_{0.95}Fe_{0.05}O_{2-\delta}$ (at 1550 °C) has been investigated. These oxides were synthesized by the coprecipitation method and mostly analyzed by XRD, TPR, and HRTEM (STEM). Fe cations substituted for Ce cations for the $Ce_{0.95}Fe_{0.05}O_{2-\delta}$ and $Ce_{0.75}Fe_{0.25}O_{2-\delta}$ 0.05 in the as prepared oxides, calcined at 500 °C. Heating them increased their crystallite size reaching about 100 nm for CeO_2 at 1200 °C (from ≈ 15 nm at 500 °C) and 70 nm for $Ce_{0.75}Fe_{0.25}O_{2-\delta}$ at 1100 °C (from ≈ 6 nm at 500 °C). HR STEM and EELS for the as prepared catalysts (calcined at 500 °C) showed, in line with XRD results, that Fe cations are homogeneously distributed inside CeO_2 . After reaction both CeO_2 and $Ce_{0.95}Fe_{0.05}O_{2-\delta}$ showed considerable growth of the crystallites (reaching sizes close to 1 μm). Part of Fe cations segregated to the edges of the crystals, forming Fe oxides, although no detachment from CeO_2 was seen. Hydrogen production was found to be equal to $2.53 \times 10^{-4} \text{ mol}(H_2) g_{\text{oxide}}^{-1}$ on $Ce_{0.95}Fe_{0.05}O_{2-\delta}$ which was 1.8 times higher than that observed on CeO_2 . The decay part of the production could be modelled by a biexponential decay function. The time constants τ_1 and τ_2 for $Ce_{0.95}Fe_{0.05}O_{2-\delta}$ were larger than for CeO_2 , indicating faster kinetics, although their ratio (τ_2/τ_1) was found to be constant. We attribute τ_1 to surface and near surface reaction and τ_2 to bulk driven reaction. The activation energy, extracted from TPR experiments, for surface reduction was found to be slightly higher (1.58 eV) than that of bulk reduction (1.43 eV) using the Kissinger method, which is in line with theoretically computed results by others.^[29] A three step mechanism of the water reaction is discussed in which the dissociative adsorption, the bulk diffusion of oxygen anions, and the hydrogen re combinative desorption are discussed. While the results point out to the role of $Ce-O-Fe$ sites in improving the reaction kinetics, the considerable sintering after one cycle indicates that maintaining oxide homogeneity is needed for long term stability.

4. Experimental Section

Synthesis: A series of cerium/iron oxides catalysts were synthesized using the coprecipitation method to get the metal oxides. Cerium (III) nitrate hexahydrate (Sigma Aldrich) was dissolved in deionized water along with iron nitrate (Sigma Aldrich). Then ammonium hydroxide was used as a precipitating agent; ≈ 50 mL of ammonium hydroxide (70%) was added to the cerium/iron mixture while stirring vigorously until the solution reached a pH of 9–10. The precipitate was then filtered and washed using 2 L of deionized water until a neutral pH was obtained. Afterward, the material was put in an oven at 100 °C and left to dry for 2 h. The oxide/hydroxide was then crushed into a fine powder, and loaded into a crucible and calcined in air at 500 °C for 12 h with a temperature ramp of 15 °C min^{-1} . A series of $Ce_xFe_{1-x}O_2$ oxides were prepared with $x = 0, 0.25, 0.75, 0.95, 1.0$ (three of them are presented in this work).

The prepared oxides were characterized using XRD, TPR, TEM, and TGA (not shown), in addition to thermal water splitting for hydrogen production.

XRD: XRD intensity data sets were collected using a PANalytical EMPYREAN diffractometer in Bragg–Brentano geometry fitted with a copper tube operating at 45 kV and 40 mA and a linear position sensitive detector. The diffractometer was configured with a 0.25° diverging slit, 0.5° antiscattering slit, 2.3° soller slits, and a Ni filter. The data sets were acquired in continuous scanning mode over the 2θ range 10°–90°, using a step interval of 0.01° and a counting time of 0.5 s per step.

TPR: TPR experiments were performed in a quartz tube coupled to a TCD (AutoChem 2920, Micrometrics). All catalysts were purged with Ar for 1 h prior to the TPR experiments which were performed under constant flow of 10 vol% H_2 in Ar mixture at 10 °C min^{-1} of ramping rate and at a flow rate of 50 mL min^{-1} . The number of moles used to reduce the oxide was calculated from the amount of H_2 consumed that was precalibrated using Ag_2O as a standard. The extraction of the activation energy for reduction of CeO_2 was conducted via two methods, commonly referred to as the Redhead^[33] and Kissinger^[34] methods. The mathematical expressions of both are shown in Equation (7) and (8).

$$\left[\frac{E_a}{k_B T_p} \right] + \ln \left[\frac{\beta_H}{k_B T_p^2} \right] + \ln \left[\frac{E_a}{A \theta_0^{(n-1)}} \right] \quad (\text{Redhead}) \quad (7)$$

$$\ln \left[\frac{\beta_H}{T_{\max}^2} \right] + \ln \left[\frac{E_a}{AR} \right] + \ln \left[\frac{E_a}{RT_{\max}} \right] + \ln \left[\frac{df(\alpha)}{d\alpha} \right]_{T=T_{\max}} \quad (\text{Kissinger}) \quad (8)$$

TEM and EELS: Electron microscopy studies were performed using Titan ST microscope (FEI company) operated at an accelerating voltage of 300 kV equipped with a field emission electron gun, a 4 k × 4 k CCD camera, a Gatan imaging filter (GIF), and Gatan microscopy suite (GMS). The microscope was operated either in HRTEM (phase contrast) or high angle annular dark field (HAADF) STEM mode (Z contrast) with point to point resolution of ≈ 0.12 nm and the information limit of ≈ 0.10 nm in both cases. HRTEM and STEM beam focus were 100 and 1.0 nm, respectively. To prepare TEM sample grid for analysis, a few mg of the oxide was dispersed in ethanol followed by ultrasonication for 15 min. A drop of supernatant suspension was poured onto a holey carbon coated Cu grid placed on a filter paper and allowed to dry. A double tilt sample holder was used to facilitate the analysis. Sample particles sitting on holes were selected for analysis where possible. EDX analysis was performed at 14° sample holder tilt angle to maximize the X rays collection in STEM mode of operation. GIF allows spectrum imaging (SI) from data collected in a synchronized STEM mode and EELS. STEM EELS was obtained in the so called dual EELS mode which acquires low loss (signal from valence electrons) and core loss (signal from core shell electrons) EELS spectra simultaneously using a high speed electrostatic shutter. The core loss EELS spectra provided the energy loss edges of $Fe-L_{2,3}$, $Ce-M_{4,5}$, and $O-K$ at the values of (721, 708), (901, 883), and 532 eV, respectively. The entire TEM data acquisition and its postprocessing analyses were carried using the GMS version 3.2 package.

Thermal Water Splitting Reaction: Because of the high temperature used, additional care was considered in constructing and testing the reactor for the thermal water splitting experiments. The system consisted of a Carbolite high temperature vertical tubular reactor type VST/1700 (up to 1700 °C) connected to a water bubbler and all lines were heated, using electric tapes, to about 120 °C. Before starting the water splitting reaction, the water container was purged with N₂ gas to remove any air bubbles out of the system to the exhaust. Afterward, the complete system was fully purged with N₂ gas multiple times. A pellet of the oxide (2.5 g with 20 mm diameter) was placed in the middle of the tubular reactor (a 1.2 m alumina tube with 3 cm inner diameter). The total reaction consists of two cycles. The first is where the catalyst sample is reduced, by increasing the tube temperature to ≈1550 °C under zero N₂ carrier. Once the oxide was reduced, the temperature of the tube reactor is decreased to ≈1200 °C before the second cycle started in which the N₂ gas (50 mL min⁻¹) was passed through the water container (kept at 80 °C). A cold water trap at the reactor exit was used prior to gas analysis. The H₂ and O₂ production amounts were measured using two gas chromatographs (the first contains a packed Molecular Sieve 5A column, 2 m long with an outer diameter of 1/8 in., with He carrier gas for O₂ and the second contains a packed Porapak Q, 2 m long with an outer diameter of 1/8 in., with N₂ as a carrier gas for H₂) with respect to time through the gas sampling 6 way valves. In the initial phase of the work, CeO₂ alone was used to optimize the reaction conditions. A total of 17 runs were conducted in which the amount of CeO₂ was changed, in addition to repeated runs with the same loading. As observed by others,^[1,13] marginal deviations from run to run were noted and the production scaled with the amount of CeO₂ used. For example, for a two consecutive runs of CeO₂ with a loading of 4.2 g, the hydrogen production per g of CeO₂ was reproducible with an error of ±7%.

Acknowledgements

The authors thank Y. Al Salik for the catalyst preparation and for providing his help during the thermochemical water splitting experiments.

Conflict of Interest

The authors declare no conflict of interest.

Data Availability Statement

Research data are not shared.

Keywords

Ce_{1-x}Fe_xO₂ TEM, Ce_{1-x}Fe_xO₂ TPR, Ce_{1-x}Fe_xO₂ XRD, hydrogen production, thermal water splitting, reaction kinetics

- [1] C. L. Muhich, B. D. Ehrhart, I. Al Shankiti, B. J. Ward, C. B. Musgrave, A. W. Weimer, *WIREs Energy Environ.* **2016**, *5*, 261.
- [2] D. Schweke, Y. Mordehovit, M. Halabi, L. Shelly, S. Hayun, *Adv. Mater.* **2018**, *30*, 1706300.
- [3] I. Al Shankiti, Y. M. Choi, F. Al Otaibi, H. Idriss, US Patents, 23 08 2016, Patent No. 9421537, and 13 06 2017 Patent No. 9675961.
- [4] S. Chuayboon, S. Abanades, *Int. J. Hydrogen Energy* **2020**, *45*, 25783.
- [5] Y. Mao, Y. Gao, W. Dong, H. Wu, Z. Song, X. Zhao, J. Sun, W. Wang, *Appl. Energy* **2020**, *267*, 114860.
- [6] J. R. Scheffe, D. Weibel, A. Steinfeld, *Energy Fuels* **2013**, *27*, 4250.
- [7] M. E. Gálvez, R. Jacot, J. Scheffe, T. Cooper, G. Patzke, A. Steinfeld, *Phys. Chem. Chem. Phys.* **2015**, *17*, 6629.
- [8] S. L. Millican, I. Androshchuk, J. T. Tran, R. M. Trottier, A. Bayon, Y. Al Salik, H. Idriss, C. B. Musgrave, A. W. Weimer, *Chem. Eng. J.* **2020**, *401*, 126015.
- [9] C. L. Muhich, B. W. Evanko, K. C. Weston, P. Lichty, X. Liang, J. Martinek, C. B. Musgrave, A. W. Weimer, *Science* **2013**, *341*, 540.
- [10] S. Ackermann, J. R. Scheffe, A. Steinfeld, *J. Phys. Chem. C* **2014**, *118*, 5216.
- [11] S. Abanades, G. Flamant, *Sol. Energy* **2006**, *80*, 1611.
- [12] D. Arifin, A. W. Weimer, *Sol. Energy* **2018**, *160*, 178.
- [13] W. C. Chueh, C. Falter, M. Abbott, D. Scipio, P. Furler, S. M. Haile, A. Steinfeld, *Science* **2010**, *330*, 1797.
- [14] J. Scaranto, H. Idriss, *Top. Catal.* **2015**, *58*, 1443.
- [15] M. Moser, M. Pecchi, T. Fend, *Energies* **2019**, *12*, 352.
- [16] D. A. Andersson, S. I. Simak, N. V. Skorodumova, I. A. Abrikosov, B. Johansson, *Appl. Phys. Lett.* **2007**, *90*, 031909.
- [17] K. S. Kang, C. H. Kim, C. S. Park, J. W. Kim, *J. Ind. Eng. Chem.* **2007**, *13*, 657.
- [18] B. E. Hanken, C. R. Stanek, N. Grønbech Jensen, M. Asta, *Phys. Rev. B* **2011**, *84*, 085131.
- [19] Z. Gu, K. Li, S. Qing, X. Zhu, Y. Wei, Y. Lid, H. Wang, *RSC Adv.* **2014**, *4*, 47191.
- [20] A. Gupta, U. V. Waghmare, M. S. Hegde, *Chem. Mater.* **2010**, *22*, 5184.
- [21] H. Wang, Z. Qu, H. Xie, N. Maeda, L. Miao, Z. Wang, *J. Catal.* **2016**, *338*, 56.
- [22] M. Lykaki, S. Stefa, S. A. C. Carabineiro, P. K. Pandis, V. N. Stathopoulos, M. Konsolakis, *Catalysts* **2019**, *9*, 371.
- [23] S. H. Begum, C. T. Hung, Y. T. Chen, S. J. Huang, P. H. Wu, X. Han, S. B. Liu, *J. Mol. Catal. A: Chem.* **2016**, *423*, 423.
- [24] T. Dhanni, S. Jayalekshmi, M. C. S. Kumar, T. P. Rao, A. C. Bose, *J. Phys. Chem. Solids* **2010**, *71*, 1020.
- [25] G. D. Takalkara, R. R. Bhosale, A. Kumara, F. AlMomania, M. Khraisheh, R. A. Shakoob, R. B. Gupta, *Sol. Energy* **2018**, *172*, 204.
- [26] I. Al Shankiti, F. Al Otaibi, Y. Al Salik, H. Idriss, *Top. Catal.* **2013**, *56*, 1129.
- [27] M. Moser, M. Pecchi, T. Fend, *Energies* **2019**, *12*, 352.
- [28] M. Fronzi, A. Soon, B. Delley, E. Traversa, C. Stampfl, *J. Chem. Phys.* **2009**, *131*, 104701.
- [29] Z. K. Han, L. Zhang, M. Liu, M. Verónica Ganduglia Pirovano, Y. Gao, *Front. Chem.* **2019**, *7*, 1.
- [30] D. Arifin, A. Ambrosini, S. A. Wilson, B. Mandal, C. L. Muhich, A. W. Weimer, *Int. J. Hydrogen Energy* **2020**, *45*, 160.
- [31] D. R. Mullins, P. M. Albrecht, T. L. Chen, F. C. Calaza, M. D. Biegalski, H. M. Christen, S. H. Overbury, *J. Phys. Chem. C* **2012**, *116*, 19419.
- [32] S. Fuente, M. M. Branda, F. Illas, *Theor. Chem. Acc.* **2012**, *131*, 19.
- [33] P. A. Redhead, *Vacuum* **1962**, *12*, 203.
- [34] H. E. Kissinger, *Anal. Chem.* **1957**, *29*, 1702.

Repository KITopen

Dies ist ein Postprint/begutachtetes Manuskript.

Empfohlene Zitierung:

Al-Taweel, S.; Nadeem, M. A.; Idriss, H.

[A Study of \$Ce_xFe_{1-x}O_2\$ as a Reducible Oxide for the Thermal Hydrogen Production from Water](#)

2022. Energy Technology, 10

[doi: 10.554/IR/1000138687](#)

Zitierung der Originalveröffentlichung:

Al-Taweel, S.; Nadeem, M. A.; Idriss, H.

[A Study of \$Ce_xFe_{1-x}O_2\$ as a Reducible Oxide for the Thermal Hydrogen Production from Water](#)

2022. Energy Technology, 10 (1), Art.Nr. 2100491.

[doi:10.1002/ente.202100491](#)

Lizenzinformationen: [KITopen-Lizenz](#)